Ocean Sci. Discuss., 6, 2341–2356, 2009
www.ocean-sci-discuss.net/6/2341/2009/

Ocean Science Discussions

Papers published in *Ocean Science Discussions* are under open-access review for the journal *Ocean Science*

First images and orientation of internal waves from a 3-D seismic oceanography data set

T. M. Blacic and W. S. Holbrook

University of Wyoming, Geology and Geophysics Department, 1000 E. University Ave., Laramie, WY, 82071, USA

Received: 11 September 2009 – Accepted: 10 October 2009 – Published: 20 October 2009

Correspondence to: T. M. Blacic (tblacic@uwyo.edu)

Published by Copernicus Publications on behalf of the European Geosciences Union.

Abstract

We present 3-D images of ocean finestructure from a unique industry-collected 3-D multichannel seismic dataset from the Gulf of Mexico that includes expendable bathythermograpgh casts for both swaths. 2-D processing reveals strong laterally continuous reflectors throughout the upper ~800 m as well as a few weaker but still distinct reflectors as deep as ~1100 m. Two bright reflections are traced across the 225-m-wide swath to produce reflector surface images that show the 3-D structure of internal waves. We show that the orientation of internal wave crests can be obtained by calculating the orientations of contours of reflector relief. Preliminary 3-D processing further illustrates the potential of 3-D seismic data in interpreting images of oceanic features such as internal wave strains. This work demonstrates the viability of imaging oceanic finestructure in 3-D and shows that, beyond simply providing a way to see what oceanic finestructure looks like, quantitative information such as the spatial orientation of features like internal waves and solitons can be obtained from 3-D seismic images. We expect complete, optimized 3-D processing to improve both the signal to noise ratio and spatial resolution of our images resulting in increased options for analysis and interpretation.

1 Introduction

Ocean mixing processes are fundamentally 3-D in nature and vary in time on a wide range of scales. Features that affect thermohaline finestructure, such as internal waves, tidal beams, solitons, eddies, fronts, warm core rings, and turbulent patches, are expected to vary in both space and time. To study these kinds of features, oceanographers typically use a combination of surface measurements (e.g., satellite sea surface elevation and surface temperature; Egbert et al., 1994; Ikeda and Emery, 1984), vertical profiles (by expendable instruments, non-expendable lowered instruments, or moored instrument arrays; e.g., Cooper et al., 1990; Rudnick et al., 2003), and towed

OSD

6, 2341–2356, 2009

instruments that can take measurements either along one horizontal line or in a "towyo" sawtooth pattern (e.g., Rudnick and Ferrari, 1999; Klymak and Moum, 2007). These methods can capture large-scale patterns over a wide area or fine-scale patterns at a discrete location or depth. High frequency (100 kHz to 1 MHz) sonar methods can provide 2-D images of backscattering in the upper ocean, which are interpreted to result from zooplankton, suspended sediment or sound-speed microstructure, and are used to map internal waves at shallow depths (e.g., Wiebe et al., 1997; Farmer and Armi, 1999). This array of measurement techniques leaves a large portion of the ocean (i.e., depths below a few hundred meters) under-sampled both laterally and vertically and opens the door to new ways of mapping oceanic fine structure.

Recently, a new method for studying the ocean has emerged called seismic oceanography. In this method, scientists process conventional low frequency (10 to 100 Hz) multichannel seismic (MCS) data to focus on imaging reflectors in the water column instead of below the sea floor (Holbrook et al., 2003). The reflectors in the water column have been shown by Nandi et al. (2004) to arise from water temperature fluctuations as small as 0.03°C. Although the images obtained can be intrinsically revealing of ocean structure, concurrent hydrographic measures (temperature/salinity profiles) are needed to ground truth the temperature variations highlighted by the reflectors. Thus far, only 2-D seismic profiles have been processed for seismic oceanography (e.g., Holbrook et al., 2003; Tsuji et al., 2005; Nakamura et al., 2006; Biescas et al., 2008), although it is now standard in the oil industry to collect 3-D seismic data using ships that tow up to seventeen parallel hydrophone streamers. Here we present the first 3-D images of ocean finestructure obtained from a data set collected by a large oil company that includes concurrent expendable bathythermograph (XBT) profiles. This industry data set may be the first of its kind with coincident seismic and water temperature measurements and represents an important step towards increasing cooperation and data sharing with the oil industry.

OSD

6, 2341–2356, 2009

2 Methods

The data set consists of two 8-cable, 2-source 3-D swaths in the Gulf of Mexico off the coast of Texas that overlap in space and are separated in time by approximately two days. Swath S168, 20.3 km in length, was collected on 2 February 2006, and swath S170, 19.0 km in length, was collected on 4 February 2006. Both were collected from NW to SE (Fig. 1). The seismic ship towed an array of 8 streamers spaced 60 m apart, each 4.65 km in length. Channel spacing along the streamers was 12.5 m; source spacing was 25 m for both sources with a flip-flop pattern (50 m when a single source is considered). This geometry results in common midpoint traces (CMPs) spaced every 6.25 m, representing the horizontal sample spacing of the resulting image in the along-swath direction. Across-swath sample spacing is determined by the source and receiver configuration. When each source is considered separately the sampled swath is 225 m wide, with an across-swath sample spacing of 15 m.

Eight expendable bathythermographs (XBTs) were deployed for each swath (Fig. 1). Casts were made from a second ship following the tail buoys at the end of the hydrophone streamers towed by the seismic vessel. The XBTs were launched to coincide with certain shot points in the seismic data in order to achieve a uniform spacing. Temperature profiles for the XBTs coinciding with swath S170 are shown in Fig. 2.

For a first look at our 3-D data set we focus on swath S170, processing each of the eight cables as individual 2-D lines for each of the two sources, thus yielding 16 parallel seismic profiles (images). To mitigate the effect of streamer feathering we only use the near 32 traces for each shot-cable pair. This results in a stacking fold of 4 and images that are noisier compared to full-fold images. However, even with this low fold we find that we can still discern strong continuous reflectors in the water. We used a standard processing flow for the seismic data that included: applying a nominal geometry layout to the data, removal of coherent and random noise, filtering in the frequency-wavenumber domain, sorting into CMP gathers, band pass frequency filtering, normal moveout, median stacking, and extended Stolt (time) migration. Since there was little

OSD
6, 2341–2356, 2009

variation in the temperature profiles from the XBTs (see Fig. 2 for temperature profiles for swath S170; profiles for S168 looked very similar), we chose the sound speed profile from XBT 2886, swath S168 to create the smoothed root mean square (RMS) sound speed profile which was used to correct traces to zero offset (i.e., normal moveout) for all cables and sources. Although using RMS sound speeds as stacking velocities can result in problems in the earth where seismic speeds can vary greatly over short depth intervals, in the ocean sound speed variation is comparatively small, thus resulting in little difference between stacked images using RMS sound speeds and hand-picked stacking velocities (Fortin and Holbrook, 2009). In addition, we limit CMP gathers to near offsets which effectively eliminates the negative effect of using RMS sound speeds to apply normal moveout. In the figures, two way time has been converted to depth assuming a constant sound speed of 1500 m/s corresponding to the average sound speed in the upper half of the water column.

We can estimate the resolution of our 2-D migrated images in the along-swath direction by considering the horizontal sample spacing. Sampling theory states that the smallest wavelength we can expect to distinguish, λ_n, (without taking noise into account) is two times the receiver spacing (Sheriff and Geldart, 1995), which for our survey geometry results in λ_n=25 m. In the across-swath direction we must consider the Fresnel zone to limit our resolution since migration was only carried out in the along-swath direction. For water depths between 300 and 1100 m, airgun sources with a dominant frequency of 20 Hz, and assuming a sound speed of 1500 m/s in the water, the first Fresnel zone ranges from 106 to 205 m. Thus, we can discern features with wavelengths somewhat smaller than the swath width, depending on the depth of the reflector. 3-D processing can improve the signal to noise ratio of the entire image volume, and with trace interpolation in the cross-swath direction and trace padding to reduce edge effects, 3-D migration can improve the resolution limit in both along-swath and cross-swath directions to be on the order of twice the receiver spacing. Vertical resolution can be estimated as a quarter of the wavelength of the highest frequency of the data (Widess, 1973). For our data, reflections have a frequency range of 30–100 Hz.

OSD

6, 2341–2356, 2009

Assuming a sound speed of 1500 m/s results in a vertical resolution of ∼4 m.

We have also performed a rudimentary stack of the entire 3-D data volume for swath S170. This initial processing consisted only of 3-D grid application, reduction of coherent and random noise, flex binning, normal moveout (using the same sound speed profile as in our 2-D processing), band pass frequency filtering and median stacking. Because 3-D migration has not yet been performed, the Fresnel zone limits the horizontal resolution of the resulting image volume to ∼100–200 m in all directions, however we can still gain some insight into the potential of 3-D seismic data sets for interpretation of oceanic processes from this first pass through a basic 3-D data processing flow.

3 Results and discussion

In this data set, strong continuous reflections are concentrated in the upper ∼800 m (Fig. 3a) with a few weaker but still discernable reflections as deep as ∼1100 m. These subhorizontal reflections most likely come from internal wave strains within the thermocline. In our current scheme using the 2-D lines it is necessary to find reflectors that can be tracked across the entire swath (i.e., that are visible and continuous in all 16 migrated images) over the same in-line distance interval in order to make a reflector surface. We chose two strong and relatively long reflectors to make example surface plots. The black box in Fig. 3a outlines the area containing the chosen reflectors, and the inset shows the tracked reflectors within this box with the two chosen reflectors highlighted in pink. We refer to the deeper reflector as reflector 1 and the shallower reflector as reflector 2. Reflector 1 was tracked across the swath from along-swath distance X=9.2 to 10.9 km; reflector 2 was tracked from X=10.6 to 13.0 km. The "flying carpet" surface images that result from combining the 16 2-D reflector tracks are shown in Fig. 3b. Reflector 2 shows a greater degree of depth variability compared to reflector 1, but the 3-D nature of both reflectors can be easily discerned. In general, the reflectors display an egg carton-like surface of peaks and troughs, though some

OSD
6, 2341–2356, 2009

features have a more linear appearance.

Orientation of internal waves that are more linear in appearance can be determined either by hand or by generating a histogram of wave contour orientations. For example, we can fit a line by eye to the wave crest in reflector 2 between 12 and 12.5 km in the along-swath direction. Knowing that the azimuth of the seismic swath is ~ 134° gives us an azimuth of 349±5° for this wave crest. More rigorously, we can draw contours of wave relief and determine the orientation of each contour line segment, as shown in Fig. 4. Here we again focus on the portion of reflector 2 between 12 and 12.5 km along the swath. Before contouring, the data is first smoothed in the across-swath direction by applying a three point moving average filter. Orientations for the contour line segments are then weighted by line segment length and plotted in a rose diagram in Fig. 4b, which shows that the dominant direction of the feature is 60–70° from the across-swath direction, or 334–344° azimuth. We note that lack of migration in the across-swath direction does not affect this determination of wave orientation. Although the across-swath resolution of the image would be improved to ~60 m with migration, this would have only a small effect on the location of the peaks and troughs and thus only a small effect on the orientation of the contour lines drawn. Therefore, measuring wave orientations is an important application of 3-D seismic oceanography images even when migration of the data is not performed. However, due to the increase in noise in the rose diagram when multiple features are included in the contouring, this method of determining wave orientation is best suited to easily discernable targets such as solitary waves and fronts.

The location, orientation, and timing of this survey was essentially random from an oceanographic perspective; both location and orientation were chosen to best suit the objectives of sub-sea floor exploration required by the oil company rather than to investigate any specific oceanic features, and timing was simply the result of the overall survey schedule rather than being set to coincide with tides or any seasonal events. However, in spite of this we find that we are still able to image some interesting oceanic features, namely, internal wave strains that cause temperature steps within the

OSD
6, 2341–2356, 2009

thermocline. Note that here we define "strain" following Thorpe (2005) as the vertical distance between two given isopycnal surfaces divided by their mean separation, and not in the formal sense of the strain tensor in an incompressible fluid. In this sense, a propagating internal wave causes zones of intensified or weakened "strain" (Thorpe, 2005, p. 60). The specific temperature variations that are the likely causes of reflectors 1 and 2 are highlighted by the inset in Fig. 2, which shows a close up of a portion of the temperature profile from the XBT cast closest to the location of our chosen reflectors, XBT 3616. Reflector 1 appears to be the result of a relatively large temperature step while reflector 2 was likely generated by a small temperature inversion.

The next step is to perform full 3-D processing of the data from both swaths including migration. This will place all CMP traces into grid boxes based on location, which will mitigate the streamer feathering problem and allow for greater and more uniform stacking fold. In general, once the stacking procedure has been optimized and 3-D migration has been performed, we expect to see an increase in the signal to noise ratio as well as an increase in our options for imaging and interpreting the structure of internal waves in this region. As an example of the type of diagram that can be made from the full 3-D stack volume to aid in interpretation, Fig. 5 shows a plot of vertical (two way time) and horizontal slices through part of the initial 3-D stack volume. In a given horizontal slice, reflector crossings appear as black bar-like features with wider bars that extend farther in the direction of the cross-line ordinals (equivalent to the along-swath direction) corresponding to flatter reflectors. In addition to making slices through the data volume, it should also be possible to pick and plot horizons to make surfaces similar to those in Fig. 3, which were obtained from parallel 2-D images.

4 Conclusions

We have performed 2-D and basic, preliminary 3-D processing of an industry 3-D multichannel seismic data set provided by a large oil company for oceanographic analysis. The data set includes 8 XBT casts for each of two 3-D seismic swaths, allowing us to

OSD
6, 2341–2356, 2009

use a local sound speed profile in our seismic data processing. The 2-D processing of one swath resulted in 16 parallel seismic images. To illustrate the utility of 3-D seismic data in studying the ocean, we selected two relatively strong and laterally continuous reflectors that could be tracked in each of the 16 2-D images. Combining the tracks produced 3-D reflector surface images that reveal the 3-D structure of the internal wave strains captured by the seismic data. Reflector surfaces display a complex egg carton-like distribution of peaks and troughs. The orientation of the more linear wave crests and troughs can be determined relative to the known azimuth of the seismic swath by plotting a histogram of wave height contour line orientations. Results of a first pass through a basic 3-D processing flow provide additional insight into the potential of 3-D data to aid in the interpretation of seismic images of ocean features such as internal wave strains. We expect full, optimized 3-D processing of the data to result in improved signal to noise ratio in the images and increased options for imaging and interpreting 3-D structures in the ocean.

This preliminary work demonstrates the viability of 3-D imaging of ocean structures as well as the feasibility of obtaining quantitative measures such as the orientation of structures from these images. The setting of the data set used in this study was essentially random as it was chosen based on industry interest in a petroleum prospect rather than on oceanographic interest. However, despite this the images of internal wave strains we obtained suggest that more dramatic results can be obtained by applying 3-D seismic imaging to specific oceanic targets such as solitary waves, eddies, fronts, and lee waves. Indeed, such focused targets that can be characterized by ~225-m-wide image slices are the best targets for this method as multiple swaths cannot be combined into a single image volume due to the time gap between swaths (on the order of hours) and the dynamic nature of oceanic features. However, multiple swaths over the same area could be compared to obtain time-lapse images of the target for studying the evolution of a feature over hours or days.

OSD

6, 2341–2356, 2009

Acknowledgements. 2-D and 3-D seismic processing was carried out using the Omega2 program package from Western Geco. Figures shown in this paper were created using the Generic Mapping Tools software (Wessel and Smith, 1991), Matlab, and The Kingdom Suite.

References

Biescas, B., Sallarès, V., Pelegrí, J. L., Machín, F., Carbonell, R., Buffet, G., Dañobeitia, J. J., and Calahorrano, A.: Imaging meddy finestructure using multichannel seismic reflection data, Geophys. Res. Lett., 35, L11609, doi:10.1029/2008GL033971, 2008.

Cooper, C., Forristall, G. Z., and Joyce, T. M.: Velocity and hydrographic structure of two Gulf of Mexico warm-core rings, J. Geophys. Res., 95(C2), 1663–1679, 1990.

Egbert, G. D., Bennett, A. F., and Foreman, M. G. G.: TOPEX/POSEIDON tides estimated using a global inverse model, J. Geophys. Res., 99(C12), 24821–24852, 1994.

Farmer, D. and Armi L.: The generation and trapping of solitary waves over topography, Science, 283(5399), 188–190, 1999.

Fortin, W. F. J., and W. S. Holbrook, Sound speed requirements for optimal imaging of seismic oceanography data, Geophys. Res. Lett., 36, L00D01, doi:10.1029/2009GL038991, 2009.

Holbrook, W. S., Paramo, P., Pearse S. and Schmitt, R. W.: Thermohaline fine structure in an oceanographic front from seismic reflection profiling, Science, 301, 821–824, 2003.

Ikeda, M. and Emery, W. J.: Satellite observations and modeling of meanders in the California Current system off Oregon and northern California, J. Phys. Oceanogr., 14(9), 1434–1450, 1984.

Klymak, J. M. and Moum, J. N.: Oceanic Isopycnal Slope Spectra: Part I – Internal Waves, J. Phys. Oceanogr., 37(5), 1215–1231, 2007.

Nakamura, Y., Noguchi T., Tsuji T., Itoh S., Niino H., and Matsuoka T.: Simultaneous seismic reflection and physical oceanographic observations of oceanic fine structure in the Kuroshio extension front, Geophys. Res. Lett., 33, L23605, doi:10.01029/2006GL027437, 2006.

Nandi, P., Holbrook, W. S., Pearse, S., Paramo, P., and Schmitt, R. W.: Seismic reflection imaging of water mass boundaries in the Norwegian Sea, Geophys. Res. Lett., 31, L23311, doi:10.1029/2204GL021325, 2004.

Rudnick, D. L. and Ferrari, R.: Compensation of horizontal temperature and salinity gradients in the ocean mixed layer, Science, 283, 526–529, 1999.

Rudnick, D. L., Boyd, T. J., Brainard, R. E., Carter, G. S., Egbert, G. D., Gregg, M. C., Holloway, P. E., Klymak, J. M., Kunze, E., Lee, C. M., Levine, M. D., Luther, D. S., Martin, J. P., Merrifield, M. A., Moum, J. N., Nash, J. D., Pinkel, R., Rainville, L., and Sanford, T. B.: From tides to mixing along the Hawaiian Ridge, Science, 301, 355–357, 2003.

Sheriff, R. E. and Geldart, L. P.: Exploration Seismology, Cambridge University Press, Cambridge, UK, 1994.

Smith, W. H. F. and Sandwell, D. T.: Global seafloor topography from satellite altimetry and ship depth soundings, Science, 277, 1957–1962, 1997.

Thorpe, S. A.: The Turbulent Ocean, Cambridge University Press, Cambridge, UK, 2005.

Tsuji, T., Noguchi, T., Niino, H., Matsuoka, T., Nakamura, Y., Tokuyama, H., Kuramoto, S., and Bangs, N.: Two-dimensional mapping of fine structures in the Kuroshio Current using seismic reflection data, Geophys. Res. Lett., 32, L14609, doi:10.1029/2005GL023095, 2005.

Wessel, P. and Smith W.: Free software helps maps and display data, EOS, 72, p. 441, 1991.

Widess, M.: How thin is a thin bed?, Geophysics, 38, 1176–1180, 1973.

Wiebe, P. H., Stanton, T. K., Benfield, M. C., Mountain, D. G., and Greene, C. H.: High-frequency acoustic volume backscattering in the Georges Bank coastal region and its interpretation using scattering models, Ocean J. Eng., 22(3), 445–464, 1997.

OSD

6, 2341–2356, 2009

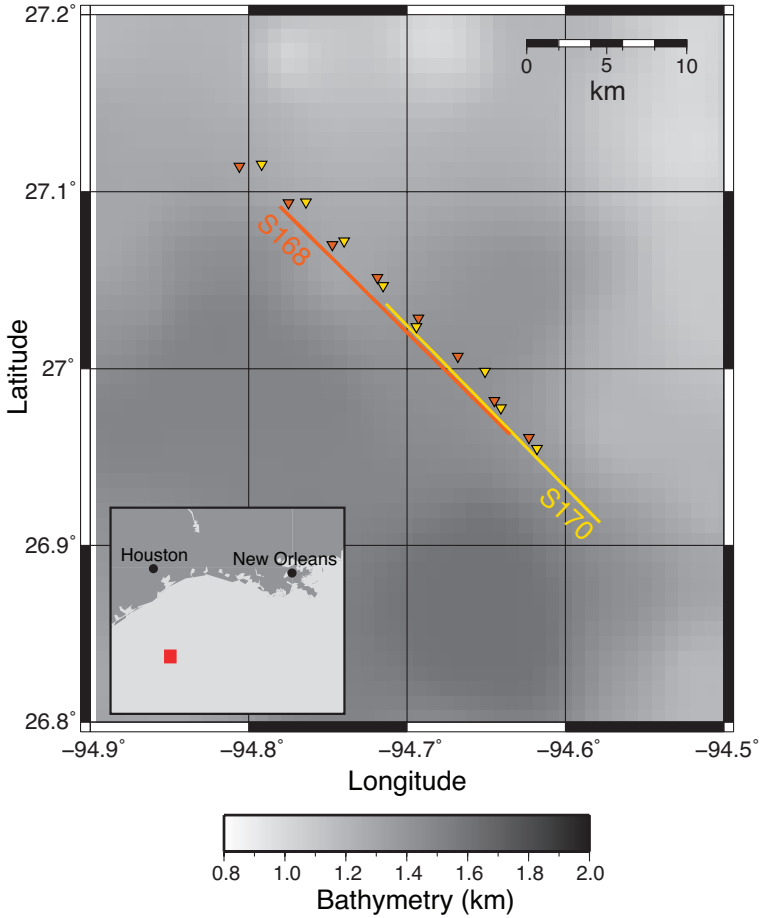

Fig. 1. Location map. Bathymetry has been interpolated from a 1′ grid (Smith and Sandwell, 1997) to 0.5′ grid spacing. Colored lines show locations of the CMP swaths; triangles show locations of the XBT casts.

OSD

6, 2341–2356, 2009

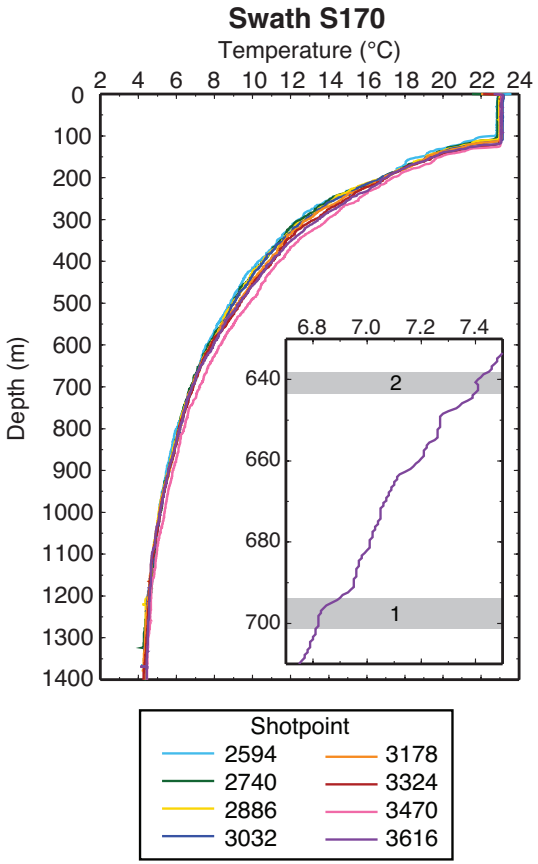

Fig. 2. Temperature profiles from XBT casts for swath S170. Inset shows blow-up of a portion of the profile for the XBT deployed nearest to the features shown in Fig. 3 (shotpoint 3616, ~0.7 km from features in Fig. 3). Grey bars highlight a temperature stair step (feature 1) and a small inversion (feature 2) which correspond with the reflector surfaces shown in Fig. 3.

OSD
6, 2341–2356, 2009

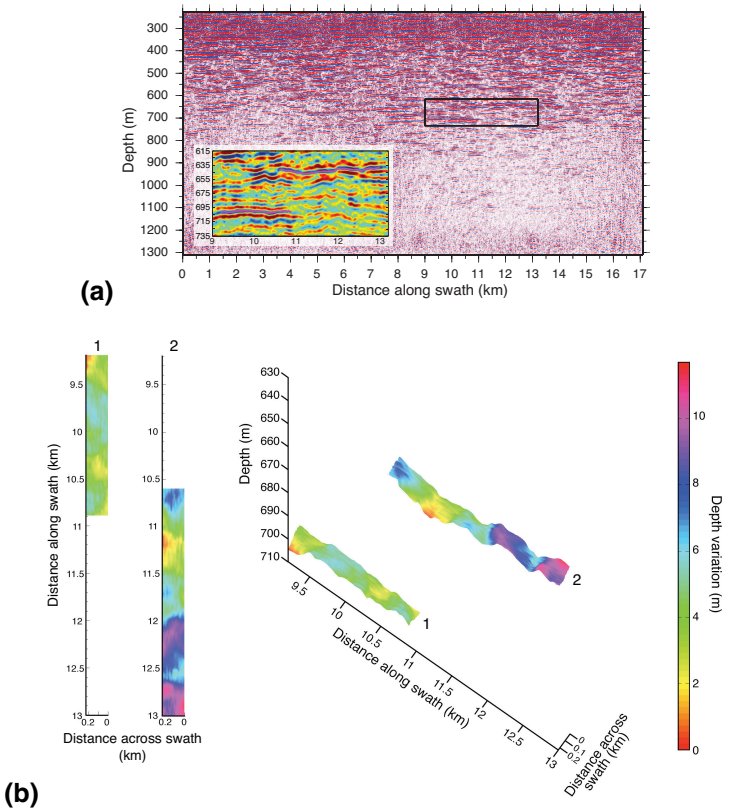

Fig. 3. Two strong continuous reflectors (highlighted as pink lines in the inset in (a)) were tracked across the swath to make reflector surfaces that illustrate the 3-D structure of the features that produced these reflections. **(a)** Migrated image of swath S170, cable 4, source 1. The images have been strongly smoothed but no relative gain control has been applied. Black box outlines region shown in the inset. **(b)** Map and 3-D view of the two reflector surfaces.

OSD
6, 2341–2356, 2009

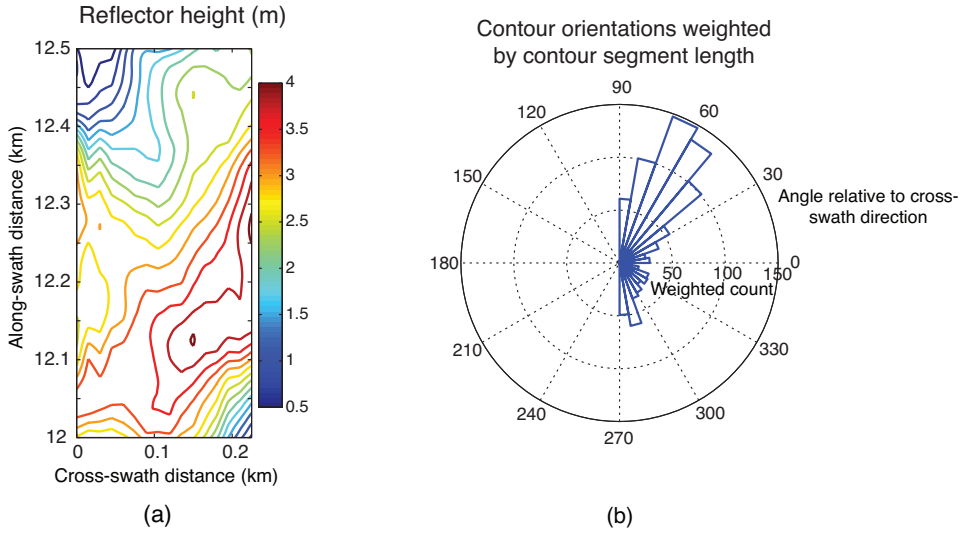

Fig. 4. Internal wave orientation can be obtained from a topographic contour plot of tracked reflectors such as those shown in Fig. 3b. **(a)** Contour plot of reflector relief for a portion of reflector 2 (see Fig. 3b). **(b)** Rose diagram showing orientations of contour line segments relative to the cross-swath direction. Histogram count has been weighted by line segment length.

OSD
6, 2341–2356, 2009

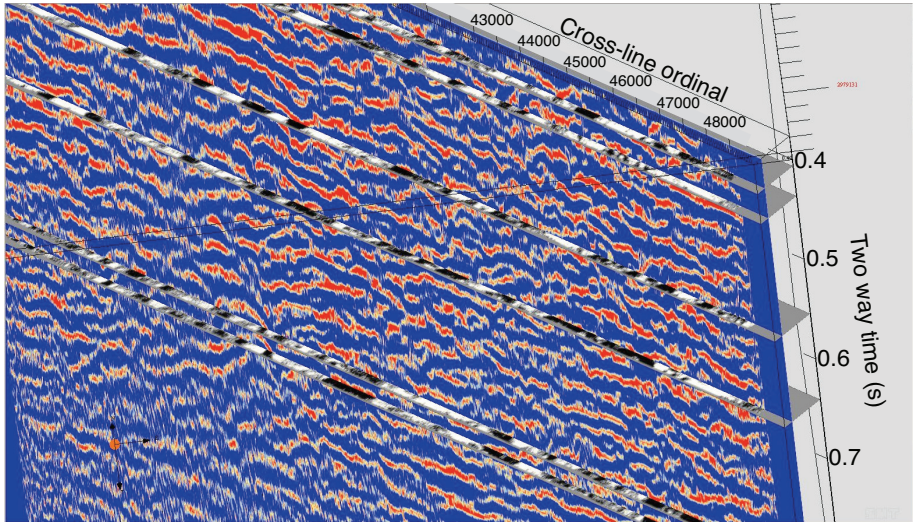

Fig. 5. 3-D view of vertical (color) and horizontal (black and white) slices through the 3-D stack volume. Data is un-migrated and a uniform gain has been applied. Cross-line ordinals denote the grid boxes in the along-swath direction.

OSD

6, 2341–2356, 2009